

# UC Santa Barbara

## UC Santa Barbara Previously Published Works

### Title

Anisotropic Growth of TiO<sub>2</sub> onto Gold Nanorods for Plasmon-Enhanced Hydrogen Production from Water Reduction

### Permalink

<https://escholarship.org/uc/item/9bf7903g>

### Journal

Journal of the American Chemical Society, 138(4)

### ISSN

0002-7863

### Authors

Wu, Binghui  
Liu, Deyu  
Mubeen, Syed  
[et al.](#)

### Publication Date

2016-02-03

### DOI

10.1021/jacs.5b11341

### Copyright Information

This work is made available under the terms of a Creative Commons Attribution-NonCommercial-NoDerivatives License, available at <https://creativecommons.org/licenses/by-nc-nd/4.0/>

Peer reviewed

# Anisotropic Growth of TiO<sub>2</sub> onto Au Nanorods for Plasmon-Enhanced Hydrogen Production from Water Reduction

Binghui Wu,<sup>†,‡,§</sup> Deyu Liu,<sup>†,§</sup> Syed Mubeen,<sup>†,#</sup> Tracy T Chuong,<sup>†</sup> Martin Moskovits,<sup>†</sup> and Galen D. Stucky<sup>†,‡,\*</sup>

<sup>†</sup>Department of Chemistry & Biochemistry, University of California, Santa Barbara, California 93106, USA

<sup>‡</sup>Collaborative Innovation Center of Chemistry for Energy Materials, Xiamen University, Xiamen 361005, China

**ABSTRACT:** Plasmonic-metal/semiconductor hetero-structures show promise as absorbers/catalysts for visible-light-driven photocatalysis. Au nanorods (AuNRs) semi-coated with TiO<sub>2</sub> are expected to be ideally structured systems for hydrogen evolution. Synthesizing such structures by wet-chemistry methods, however, has proved challenging. Here we report the bottom-up synthesis of AuNR-TiO<sub>2</sub> nanodumbbells with spatially separated gold/TiO<sub>2</sub> regions, whose structures are governed by the NRs' diameter, and the higher curvature and lower density of C<sub>n</sub>TAB surfactant at the NRs' tips than on their lateral surfaces, as well as the morphology's dependence on concentration, and alkyl chain length of C<sub>n</sub>TAB. The nano-dumbbells show plasmon-enhanced hydrogen evolution under visible and near-infrared light.

Photocatalysis has received significant attention for solar conversion to electricity or fuels based on electron-hole pair production in semiconductors.<sup>1</sup> However, this process is constrained mainly by low photocatalytic efficiency and limited visible and near-infrared (NIR) photoabsorption. Efficient engineering of the photocatalyst surface and interface is crucial to overcome these limitations.<sup>2-5</sup> Recently, surface plasmon resonance (SPR) of Au,<sup>2,3,6-11</sup> Ag<sup>12-14</sup> and Pd<sup>15,16</sup> nanoparticles has been applied to efficiently enhance visible and NIR absorption and generate SPR hot electrons.<sup>4,17,18</sup>

Among these nanostructures, AuNRs with tunable SPR are of particular interest due to the fact of their wide range of light harvesting; panchromatic absorption toward the solar spectrum can significantly improve the solar energy conversion efficiency.<sup>11</sup> Moreover, AuNRs are usually interfaced with efficient electron acceptors (such as semiconductor TiO<sub>2</sub>,<sup>19</sup> graphene,<sup>20</sup> cocatalyst Pt<sup>0</sup>) to maximize the charge separation of hot electrons. Recently, we developed an autonomous, AuNR-TiO<sub>2</sub> based photocatalytic device with oxidation and reduction co-catalysts using nanofabrication techniques.<sup>3</sup> We clearly demonstrated that the plasmonic metal-semiconductor interface, which is a Schottky junction, can effectively select out the hot electrons; so that all charge carriers involved in the oxidation and reduction steps arise from these hot electrons, which are generated by the excitation of surface plasmons in the nanostructured AuNRs. In order to realize recycling of the photo-reduction/-oxidation, extraction of the hot electrons requires both refilling of these electrons and an electron donor accessible region on the SPR metal surface.<sup>3,10,11,16,18,21-23</sup> The spatial separation structure (rather than homogenous core-shell

structure) can be provided by line-of-sight depositions using nanofabrication techniques that rely on advanced facilities and sophisticated operators. This nanofabrication method is usually not applicable for freestanding AuNRs synthesized by wet chemistry when there is no control of the orientation needed to create anisotropic AuNR-TiO<sub>2</sub> structures. Additionally, all wet-chemistry routes to such a well-defined spatial separation structure are challenging.

Anisotropic growth of TiO<sub>2</sub> onto AuNRs, instead of depositing AuNRs onto TiO<sub>2</sub>,<sup>24</sup> could give better contact between Au and TiO<sub>2</sub>. Because bilayers of surface-capping agents such as cetyltrimethylammonium bromide (C<sub>16</sub>TAB) are more densely packed on AuNR sides than at the tips, this phenomenon has been utilized for the anisotropic overgrowth on C<sub>16</sub>TAB-capped AuNRs with metal heterostructures or silica.<sup>7,9,25</sup> However, anisotropic overgrowth of semiconductors such as TiO<sub>2</sub> on C<sub>16</sub>TAB-capped AuNRs in solution has been rarely reported.<sup>26</sup>

In this study, we report a wet-chemistry method for the anisotropic overgrowth of TiO<sub>2</sub> on AuNRs by using C<sub>n</sub>TAB as a soft template and by controlling the degree of hydrolysis of TiCl<sub>3</sub>. The roles of concentration and alkyl chain length of C<sub>n</sub>TAB as well as the diameter of the AuNRs were carefully studied. The as-prepared TiO<sub>2</sub>-tipped AuNRs have a dumbbell and spatial separation structure, and TiO<sub>2</sub> acts as a filter for hot electrons from AuNRs. This structure satisfies the electron refilling requirement and exhibits plasmon-enhanced hydrogen production from water reduction under visible and NIR light irradiation.

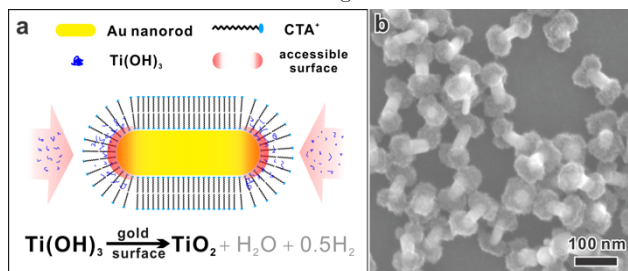


**Figure 1.** (a) Schematic showing the origin of anisotropic TiO<sub>2</sub> coating. (b) SEM image of the as-prepared AuNR-TiO<sub>2</sub> nanodumbbells. Synthetic condition: 32 nm AuNRs (in diameter), 13.9 mM C<sub>16</sub>TAB.

Figure 1a illustrates the formation of the dumbbell nanoparticles by our bottom-up wet-chemistry method. The  $C_{16}$ TAB bilayer confines the AuNR with only the tips accessible to Ti species. By controlling the hydrolysis of  $TiCl_3$  via the pH or the reaction solution with  $NaHCO_3$ ,<sup>27,28</sup>  $Ti^{3+}$  is catalytically oxidized on the Au tips to form  $TiO_2$ . Figure 1b is a typical SEM image of as-prepared AuNR- $TiO_2$  nanodumbbells using  $C_{16}$ TAB-capped AuNRs as seeds (Figure S1). The product consists of uniform nanodumbbell structures with the two tips of all the AuNRs coated with  $TiO_2$  caps and the sides exposed. During the coating process, red shifts of SPR bands are observed *in situ* in the UV-Vis spectra (Figure S2). This phenomenon corresponds to a local refractive index change due to the formation of the  $TiO_2$  caps on the AuNR, and agrees with previous reports of dielectric material coatings on Au nanoparticles.<sup>28-30</sup> Due to the release of acid during the  $TiCl_3$  hydrolysis, and the spatial coverage of the Au surface by the  $TiO_2$  deposition, the reaction slows down after about 30 min. In the synthesis, the spatial selectivity of the  $TiO_2$  deposition on the AuNRs is controlled by engineering their surface chemistry. Another type of nanoparticles, with a fully coated core-shell structure, can be prepared using a similar  $TiCl_3$  hydrolysis process with the AuNRs pre-modified by an anionic surfactant, sodium dodecyl sulfate (SDS, Figure S3).

The anisotropic overgrowth of  $TiO_2$  on AuNRs is further shown by TEM and HAADF-STEM-EDX analyses (Figure 2 and Figure S4). The micrograph reveals that the  $TiO_2$  caps are porous with basic building blocks smaller than 2 nm. The elemental mapping of the as-prepared product confirms that the two caps are made from  $TiO_2$ . The signal distribution obtained by linear scanning in the longitude direction clearly indicates the existence of two symmetrical  $TiO_2$  caps. No Ti signal has been found by transverse scanning through the lateral side, further confirming specific tip-side selectivity of the deposition. Furthermore, the significant distribution difference and shape of the caps suggest that the anisotropic deposition of  $TiO_2$  is initiated from two tips of each AuNR and then extended towards the middle side surface of AuNRs. Note that the  $TiO_2$  caps are amorphous based on the  $TiO_2$  ultrafine domain size revealed in the HRTEM and XRD patterns (Figure S5).

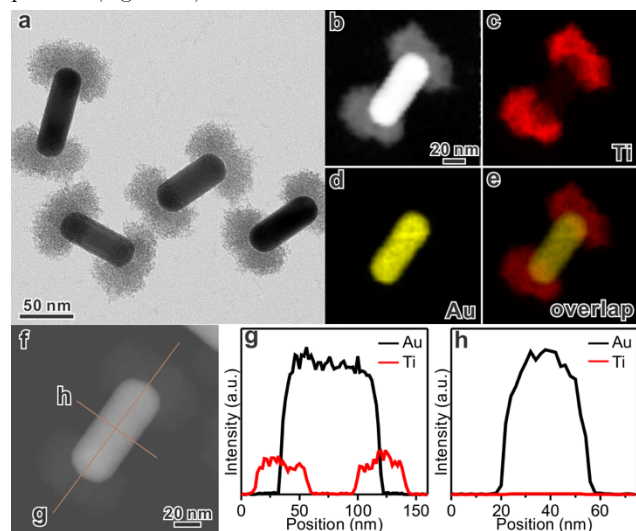


**Figure 2.** (a) TEM image, (b-e) HAADF-STEM image and elemental maps and (f-h) Au and Ti elemental profiles of AuNR- $TiO_2$  nanodumbbells.

Anisotropic overgrowth of  $TiO_2$  on the AuNR tips can be explained by the bilayer adsorption structure of  $C_{16}$ TAB and the special structure of the AuNR tips. The bilayer can behave as a soft template that guides the preferential bonding of the Au surface to solution species. Due to the curvature difference, the assembly of  $C_{16}$ TAB on both tips of AuNR is less compact than that on the side.<sup>25,31</sup> The lower obstruction in these regions allows solution species to approach the AuNR tip surface (Figure 1a). This phenomenon has been previously used for the selective surface functionalization of AuNR tips.<sup>32-34</sup> By generalizing the side/tip selective functionalization for hydrolysis reactions, Wang's group successfully prepared AuNRs with an anisotropic  $SiO_2$  or  $Ag_2O$  coating.<sup>25,35</sup> Similarly, here the  $TiO_2$  formation process (which is a hydrogen evolution reaction due to the oxidation of the  $TiCl_3$  precursor<sup>27</sup>) can be selectively catalyzed by the accessible AuNR tips, resulting in the spatially selective coating of  $TiO_2$  on AuNRs. The anisotropic overgrowth can be due to both less dense assembly of  $C_{16}$ TAB and herein less electrostatic repulsion between Ti species and the positively-charged  $C_{16}$ TAB bilayer.<sup>34,36,37</sup> In contrast, SDS or similar surfactants modified AuNRs have a more random molecular assembly on them, resulting in homogenous overgrowth of  $TiO_2$  on AuNRs.<sup>28,34</sup>

In order to gain a deeper understanding of why  $C_{16}$ TAB promoted the anisotropic growth of  $TiO_2$ , the relation between the growth and the concentration of  $C_{16}$ TAB was studied. Figure 3 and Figure S6 show the  $C_{16}$ TAB concentration effect on  $TiO_2$  growth using the same AuNRs of 32nm in diameter. In order to reach a >90% yield of AuNR-dumbbells, the  $C_{16}$ TAB concentration must be appropriate, that is, in the range between its first critical micelle concentration (1<sup>st</sup> CMC, 0.89 mM<sup>38</sup>) and its 2<sup>nd</sup> CMC (20 mM<sup>38</sup>). When  $C_{16}$ TAB concentration is lower than the 1<sup>st</sup> CMC, most of the AuNRs are fully covered with a rough  $TiO_2$  shell, due to the unstable and easily disrupted  $C_{16}$ TAB bilayer.<sup>34</sup> When the  $C_{16}$ TAB concentration is greater than the 2<sup>nd</sup> CMC, a large portion of the product has only one tip coated with  $TiO_2$ , or is not coated at all, due to the ultra-dense bilayer of  $C_{16}$ TAB. However, for concentrations of  $C_{16}$ TAB between the 1<sup>st</sup> and 2<sup>nd</sup> CMC, the deposition of  $TiO_2$  is effectively limited to two tips with a high yield. A similar result was reported by Wang et al,<sup>25</sup> i.e., an appropriate  $C_{16}$ TAB concentration (~6 mM) leads to effective overgrowth of  $SiO_2$  onto AuNR tips. These results show that a well-assembled  $C_{16}$ TAB bilayer is critical for the anisotropic overgrowth of  $TiO_2$  on AuNRs.

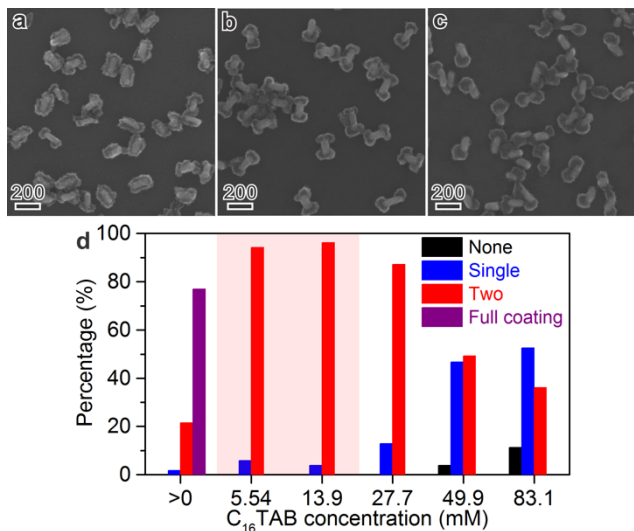


**Figure 3.** C<sub>16</sub>TAB concentration effect in TiO<sub>2</sub> growth on AuNRs. The same AuNR diameter (32 nm), but different C<sub>16</sub>TAB concentrations: (a) no additional C<sub>16</sub>TAB, (b) 5.54 mM, and (c) 83.1 mM. (d) The percentage histogram of coated AuNR tips. Note that the pink shadow indicates the C<sub>16</sub>TAB concentration between its 1<sup>st</sup> and 2<sup>nd</sup> CMC.

Based on the assumption of the relationship between the selective coating and the C<sub>16</sub>TAB bilayer, curvatures of the AuNR tips should play a critical role. AuNRs with different diameters as the seeds were used in the presence of the same C<sub>16</sub>TAB concentration. The histogram in Figure 4a shows a correlation of AuNR diameters and the percentage of coated tips in the products. The trend shows that the thinner AuNRs, the harder it is to coat TiO<sub>2</sub> on the tips of the AuNRs (regardless of their lengths). A large percentage of the products formed using narrow AuNRs (diameter smaller than 20 nm) are either coated on a single tip or are completely without coating (Figure S7). Since the curvature has a reciprocal relationship with the diameter, seemingly the C<sub>16</sub>TAB bilayer on thinner AuNRs should have a more open structure on the tips, which should allow the region to be coated more easily. On the other hand, the area on the tip of a thinner AuNR is also significantly reduced. The decreased tip area may dramatically reduce the ability of nucleating TiO<sub>2</sub> caps. For example, considering the hemisphere area on the tips of AuNRs and assuming the same TiO<sub>2</sub> coating length (10-20 nm, based on TEM analysis) from the tips along the NRs, the coated surface area will be reduced by 20-30% when the AuNR diameter is reduced from 32 to 27 nm; this obviously changes the ability to form the TiO<sub>2</sub> caps on AuNRs and their stability. As shown in Figure 4a, the onset diameter of this change is about 20 nm. In addition, Au does not have strong chemical binding to amorphous TiO<sub>2</sub>. From our observations, the overall effect of reducing the AuNR diameter is dominated by this stability aspect.

Since C<sub>16</sub>TAB cannot lead to the coating of thin AuNRs (<27 nm in diameter) to give a high yield of TiO<sub>2</sub> overgrowth, other C<sub>n</sub>TABs with shorter alkyl chain were studied. Figure 4b and Figure S8 shows the result of coating TiO<sub>2</sub> onto thin AuNRs (22

nm in diameter) in the presence of single C<sub>n</sub>TAB (x=12, 14, 16; note that the same molar concentration optimized for C<sub>16</sub>TAB were used thoroughly). The yield of tip-selective coating on thin AuNRs is significantly improved when using C<sub>14</sub>TAB or C<sub>12</sub>TAB instead of C<sub>16</sub>TAB. Their shorter hydrocarbon chains give a weaker hydrophobic interaction between molecules, so that better permit a bilayer adsorption structure on the thin AuNR tip surface. Especially on the tips of thin AuNRs, the C<sub>14</sub>TAB or C<sub>12</sub>TAB bilayer allows Ti(III) species access to the catalytic Au surface more easily in spite of the higher curvature, therefore makes a thicker TiO<sub>2</sub> deposition possible and thus compensates the instability from the smaller area on the tips of thin AuNRs. Furthermore, AuNR diameter effect in the presence of C<sub>12</sub>TAB (13.9 mM; its 1<sup>st</sup> CMC is ~14 mM<sup>39</sup>) was studied (Figure S9). For 15 nm AuNRs, C<sub>12</sub>TAB leads to higher possibility of tipped TiO<sub>2</sub> coating than C<sub>16</sub>TAB, which is converse for the case of 32 nm AuNRs. Indeed, our studies reveal that an optimum combination of C<sub>n</sub>TAB with specific carbon chain length and AuNR diameter is essential in order to obtain a high-yield anisotropic overgrowth of TiO<sub>2</sub> onto AuNR tips. Previous investigations were conducted using C<sub>18</sub>TAB or C<sub>18</sub>TAC for the overgrowth of metal heterostructures or silica on AuNRs with limited diameters<sup>7,9,25</sup>; here we focus on varying the C number in C<sub>n</sub>TAB to control the capping agent functionality in heterogeneous overgrowth processes of TiO<sub>2</sub> on AuNRs with various diameters.

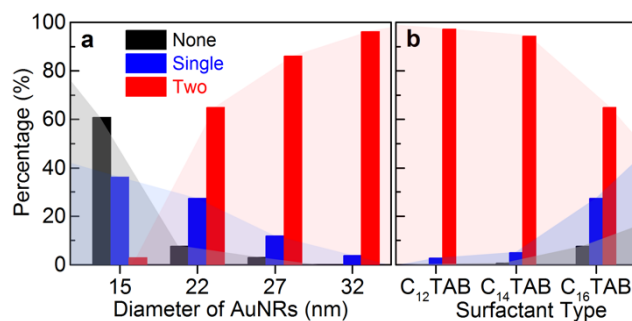


**Figure 4.** Percentage histogram of coated tips on AuNR-TiO<sub>2</sub> product synthesized under similar conditions, with (a) the same concentration of C<sub>16</sub>TAB (13.9 mM), but different AuNR diameters, and (b) same AuNR diameter (22 nm), but different C<sub>n</sub>TABs (13.9 mM).

It should be noted that mixing two C<sub>n</sub>TABs with different chain lengths (values of n) can change the growth behavior of TiO<sub>2</sub> on AuNRs when compared to growth using a single C<sub>n</sub>TAB. Figure S10 shows the product prepared in a mixed C<sub>12</sub>TAB/C<sub>16</sub>TAB (1:1) solution. In this case, TiO<sub>2</sub> is inclined to coat the sharp corners which connect the side and the endmost tips of AuNRs, rather than the whole tips as in the case of single C<sub>n</sub>TAB (Figure S7d, S9d). This is also attributed to the limitation from C<sub>n</sub>TAB bilayer structure. As a mixture of two C<sub>n</sub>TABs, the entropic force makes C<sub>16</sub>TAB with longer hydrocarbon chains (C<sub>16</sub>) go to the less curved surface and push the shorter C<sub>12</sub>TAB aside to corners. The higher percentage of shorter C<sub>12</sub>TAB on sharp corners significantly reduces the hindrance for TiO<sub>2</sub> deposition on that focused region and allows it to form small caps on the AuNR tips.

The most exciting feature of the designed AuNR-TiO<sub>2</sub> nanodumbbells is their ability to promote SPR-induced hot-electron

generation under visible and NIR light. While AuNR@TiO<sub>2</sub> core-shell nanoparticles and pure amorphous TiO<sub>2</sub> show no activity for hydrogen evolution, AuNR-TiO<sub>2</sub> nanodumbbells exhibit relatively high photoactivity, compared to physically mixed AuNRs and amorphous TiO<sub>2</sub> (Figure 5a; AuNR#5 with 32-nm diameter were used). Note that the difference in the photocatalytic activity of these three samples does not result from the surface area or the mass of TiO<sub>2</sub>, since amorphous TiO<sub>2</sub> itself does not absorb visible light and a significantly excess quantity of TiO<sub>2</sub> was used in the mechanical mixture of AuNRs and TiO<sub>2</sub>. The activity of AuNR-TiO<sub>2</sub> nanodumbbells is higher than that of spherical Au nanoparticles deposited on crystalline TiO<sub>2</sub> under similar condition.<sup>40</sup> Further increasing the crystallinity of the TiO<sub>2</sub> and adding co-catalysts could enhance the visible light performance of our AuNR-TiO<sub>2</sub> dumbbells.<sup>3</sup> These control experiments clearly demonstrate the importance of AuNR-dumbbell structure with intimate physical contact and strong plasmonic coupling for enhanced charge separation in the plasmon-enhanced photocatalysis. The difference of the photocatalytic activities under visible light for the AuNR-TiO<sub>2</sub> nanodumbbells and the AuNR@TiO<sub>2</sub> core-shell structure further suggests that the plasmon-enhanced photocatalysis mechanism is plasmonic hot electron transfer due to localized surface plasmon resonance of AuNRs (which is dependent on the configuration/architecture of metal-semiconductor heterojunction), rather than plasmon-induced resonance energy transfer (based on the inactivity of the core-shell structure).<sup>41,42</sup>

Hot electron generation was further demonstrated in the photoreduction of methylene blue (MB), a model acceptor molecule (Figure 5b). After 60 min of irradiation, the AuNR-TiO<sub>2</sub> dumbbells exhibited reduction of ~60% of the MB dye. In the control experiments, physically mixed AuNRs and TiO<sub>2</sub> solution exhibited reduction of ~10% of the MB, while AuNR@TiO<sub>2</sub> core-shell structure showed insignificant activity (<1%; moreover, part of the activity may come from photobleaching<sup>43</sup>). These experiments on the photoreduction of MB demonstrate the importance of close contact and the anisotropic assembly of the AuNR and TiO<sub>2</sub> domains for effective visible light photocatalysis.

Previous studies indicate that the SPR-induced hot electrons can be filtered out from metal nanoparticles with the positive charges left behind.<sup>3,4,11,18,34</sup> Note that neither TiO<sub>2</sub> alone nor pure AuNRs can produce hydrogen under similar conditions. For the nanodumbbells, the oxidation pathway is on their side surface (Figure 5c), where the lateral side of AuNRs can be directly exposed to electron donors so that oxidation reactions can take place. With AuNR partially exposed in the dumbbell structure, AuNRs generate a concentrated electromagnetic field that focuses energy flux around the semiconductor, and thus enhance hot-electron generation and photocatalytic activity.<sup>3,9,18,44,45</sup> As pointed out by Yates,<sup>46</sup> metal-TiO<sub>2</sub> contact induces band bending in TiO<sub>2</sub> which can be used either for electron or hole transfer, depending on whether that band bends upward or downward, which, in turn, depends on the relative ordering of the semiconductor's and metal's Fermi levels. The Fermi level of TiO<sub>2</sub> is higher than that of Au, causing the bands of the TiO<sub>2</sub> to bend upward at the interface between these two materials (at which a Schottky junction is formed). At the interface, electrons would flow "down" and holes "up" in the bent conduction band and valence band respectively, as shown in energy band diagrams.<sup>46</sup> Holes generated in AuNRs under visible light are, therefore, unlikely to transfer to TiO<sub>2</sub>. In contrast, hot electrons generated in AuNRs under visible light that overcome the Schottky barrier are likely to flow from AuNRs to TiO<sub>2</sub> and be available for photo-reduction with

TiO<sub>2</sub> acting as the electron transfer medium. The dumbbell structure ideally exploits such charge exchange opportunities, carrying out reduction processes on the TiO<sub>2</sub> then restoring charge balance to the Au core through oxidation reactions that would occur on the bare portions of the AuNRs (Figure 5c). A fully coated AuNR is denied of the opportunity for establishing such a complete circuit that allows both electrons and holes to access their appropriate reaction partners, thereby blocking the continuous flow of the hot charge carriers resulting from the excitation of the SPR (Figure 5d). We, therefore, ascribe the better SPR photocatalytic performance of the dumbbells to their ability to present appropriate and separate regions at which the oxidation and reduction processes can take place, as opposed to the core-shell nanoparticles without such separate regions.

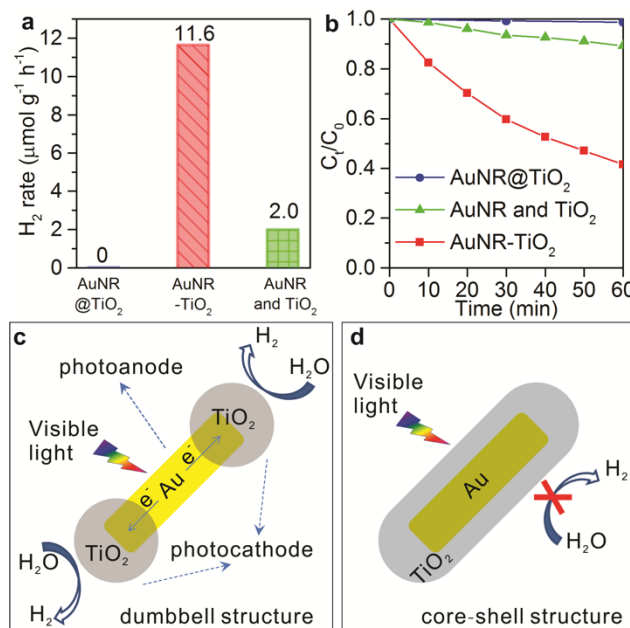


**Figure 5.** Comparison of (a) hydrogen evolution rate by various catalysts, and (b) normalized concentration of MB dye vs irradiation time; both under visible illumination and in the presence of methanol and water. (c-d) Structure and mechanism of operation under visible light of (c) an individual AuNR-TiO<sub>2</sub> dumbbell and (d) core-shell AuNR@TiO<sub>2</sub>. In (c), hot electrons generated from plasmonic AuNRs are filtered out by the Au-TiO<sub>2</sub> Schottky barrier for photo-reduction and regenerated from the electron donor (methanol here).

In summary, an easy, bottom-up, wet-chemistry technique for the synthesis of anisotropic TiO<sub>2</sub> overgrowth on AuNRs has been developed using the selective spatial assembly of a C<sub>n</sub>TAB bilayer on AuNR surfaces and the hydrolysis of TiCl<sub>4</sub>. The concentration, alkyl chain length of C<sub>n</sub>TAB, and the diameter of AuNRs are important in order to control the selective overgrowth. The as-prepared AuNR-TiO<sub>2</sub> nanodumbbells exhibit plasmon-enhanced hydrogen evolution under visible-NIR light. The created AuNR-TiO<sub>2</sub> interface with the AuNR side exposed, as a Schottky junction, can filter out SPR hot electrons from the AuNRs. Engineering the structure, such as loading co-catalysts, may further improve its activity for the plasmon-induced hydrogen evolution.

This work shows an alternative solution of anisotropic TiO<sub>2</sub> overgrowth rather than nanofabrication techniques, and is expected to be a promising platform for the development of free-standing functional photocatalysts.

## ASSOCIATED CONTENT

### Supporting Information

Experimental details, TEM, HRTEM, SEM images, XRD, UV-vis spectra. This material is available free of charge via the Internet at <http://pubs.acs.org>.

## AUTHOR INFORMATION

### Corresponding Author

\*E-mail: [stucky@chem.ucsb.edu](mailto:stucky@chem.ucsb.edu)

### Author Contributions

§These authors contributed equally.

### Present Addresses

#Department of chemical and biochemical engineering, University of Iowa, Iowa City, IA 52242, USA

### Notes

The authors declare no competing financial interests.

## ACKNOWLEDGMENT

This research was supported by the Center for Energy Efficient Materials, an Energy Frontier Research Center funded by the U.S. Department of Energy, Office of Science, Basic Energy Sciences under award no. DE-SC0001009 and by the National Science Foundation (DMR 0805148). The MRL Shared Experimental Facilities are supported by the MRSEC Program of the NSF under award no. DMR 1121053; a member of the NSF-funded Materials Research Facilities Network ([www.mrfn.org](http://www.mrfn.org)). B.W. was partially supported by China Scholarships Council for this research. We gratefully acknowledge Jialuo Li (TAMU) for help with drawing the schematic TOC figure.

## REFERENCES

- (1) Ma, Y.; Wang, X. L.; Jia, Y. S.; Chen, X. B.; Han, H. X.; Li, C. *Chem. Rev.* **2014**, *114*, 9987.
- (2) Tada, H.; Mitsui, T.; Kiyonaga, T.; Akita, T.; Tanaka, K. *Nat. Mater.* **2006**, *5*, 782.
- (3) Mubeen, S.; Lee, J.; Singh, N.; Kramer, S.; Stucky, G. D.; Moskovits, M. *Nat. Nanotechnol.* **2013**, *8*, 247.
- (4) Kochuveedu, S. T.; Jang, Y. H.; Kim, D. H. *Chem. Soc. Rev.* **2013**, *42*, 8467.
- (5) Liu, C.; Tang, J. Y.; Chen, H. M.; Liu, B.; Yang, P. D. *Nano Lett.* **2013**, *13*, 2989.
- (6) Tian, Y.; Tatsuma, T. *J. Am. Chem. Soc.* **2005**, *127*, 7632.
- (7) Wang, F.; Li, C. H.; Chen, H. J.; Jiang, R. B.; Sun, L. D.; Li, Q.; Wang, J. F.; Yu, J. C.; Yan, C. H. *J. Am. Chem. Soc.* **2013**, *135*, 5588.
- (8) Wu, K. F.; Rodriguez-Cordoba, W. E.; Yang, Y.; Lian, T. Q. *Nano Lett.* **2013**, *13*, 5255.
- (9) Zheng, Z. K.; Tachikawa, T.; Majima, T. *J. Am. Chem. Soc.* **2014**, *136*, 6870.
- (10) Moskovits, M. *Nat. Nanotechnol.* **2015**, *10*, 6.
- (11) Mubeen, S.; Lee, J.; Liu, D. Y.; Stucky, G. D.; Moskovits, M. *Nano Lett.* **2015**, *15*, 2132.
- (12) Christopher, P.; Xin, H. L.; Linic, S. *Nat. Chem.* **2011**, *3*, 467.
- (13) Li, G.; Cherqui, C.; Bigelow, N. W.; Duscher, G.; Straney, P. J.; Millstone, J. E.; Masiello, D. J.; Camden, J. P. *Nano Lett.* **2015**, *15*, 3465.
- (14) Ingram, D. B.; Linic, S. *J. Am. Chem. Soc.* **2011**, *133*, 5202.
- (15) Long, R.; Mao, K. K.; Gong, M.; Zhou, S.; Hu, J. H.; Zhi, M.; You, Y.; Bai, S.; Jiang, J.; Zhang, Q.; Wu, X. J.; Xiong, Y. J. *Angew. Chem. Int. Ed.* **2014**, *53*, 3205.
- (16) Long, R.; Rao, Z.; Mao, K.; Li, Y.; Zhang, C.; Liu, Q.; Wang, C.; Li, Z. Y.; Wu, X.; Xiong, Y. *Angew. Chem. Int. Ed.* **2015**, *54*, 2425.
- (17) Jiang, R.; Li, B.; Fang, C.; Wang, J. *Adv. Mater.* **2014**, *26*, 5274.
- (18) Clavero, C. *Nat. Photon.* **2014**, *8*, 95.
- (19) Pu, Y. C.; Wang, G. M.; Chang, K. D.; Ling, Y. C.; Lin, Y. K.; Fitzmorris, B. C.; Liu, C. M.; Lu, X. H.; Tong, Y. X.; Zhang, J. Z.; Hsu, Y. J.; Li, Y. *Nano Lett.* **2013**, *13*, 3817.
- (20) Hoggard, A.; Wang, L. Y.; Ma, L. L.; Fang, Y.; You, G.; Olson, J.; Liu, Z.; Chang, W. S.; Ajayan, P. M.; Link, S. *ACS Nano* **2013**, *7*, 11209.
- (21) Furube, A.; Du, L.; Hara, K.; Katoh, R.; Tachiya, M. *J. Am. Chem. Soc.* **2007**, *129*, 14852.
- (22) Wang, C.; Astruc, D. *Chem. Soc. Rev.* **2014**, *43*, 7188.
- (23) DuChene, J. S.; Sweeny, B. C.; Johnston-Peck, A. C.; Su, D.; Stach, E. A.; Wei, W. D. *Angew. Chem. Int. Ed.* **2014**, *53*, 7887.
- (24) Liu, L. Q.; Ouyang, S. X.; Ye, J. H. *Angew. Chem. Int. Ed.* **2013**, *52*, 6689.
- (25) Wang, F.; Cheng, S.; Bao, Z.; Wang, J. *Angew. Chem. Int. Ed.* **2013**, *52*, 10344.
- (26) Seh, Z. W.; Liu, S. H.; Zhang, S. Y.; Bharathi, M. S.; Ramanarayan, H.; Low, M.; Shah, K. W.; Zhang, Y. W.; Han, M. Y. *Angew. Chem. Int. Ed.* **2011**, *50*, 10140.
- (27) Liu, R.; Sen, A. *J. Am. Chem. Soc.* **2012**, *134*, 17505.
- (28) Fang, C. H.; Jia, H. L.; Chang, S.; Ruan, Q. F.; Wang, P.; Chen, T.; Wang, J. F. *Energ. Environ. Sci.* **2014**, *7*, 3431.
- (29) Chen, H. J.; Wang, F.; Li, K.; Woo, K. C.; Wang, J. F.; Li, Q.; Sun, L. D.; Zhang, X. X.; Lin, H. Q.; Yan, C. H. *ACS Nano* **2012**, *6*, 7162.
- (30) Li, B. X.; Gu, T.; Ming, T.; Wang, J. X.; Wang, P.; Wang, J. F.; Yu, J. C. *ACS Nano* **2014**, *8*, 8152.
- (31) Zhang, S. Z.; Kou, X. S.; Yang, Z.; Shi, Q. H.; Stucky, G. D.; Sun, L. D.; Wang, J. F.; Yan, C. H. *Chem. Commun.* **2007**, 1816.
- (32) Nie, Z. H.; Fava, D.; Kumacheva, E.; Zou, S.; Walker, G. C.; Rubinstein, M. *Nat. Mater.* **2007**, *6*, 609.
- (33) Liu, K.; Zhao, N. N.; Kumacheva, E. *Chem. Soc. Rev.* **2011**, *40*, 656.
- (34) Chen, H.; Shao, L.; Li, Q.; Wang, J. *Chem. Soc. Rev.* **2013**, *42*, 2679.
- (35) Bao, Z. H.; Sun, Z. H.; Xiao, M. D.; Chen, H. J.; Tian, L. W.; Wang, J. F. *J. Mater. Chem.* **2011**, *21*, 11537.
- (36) Perez-Juste, J.; Liz-Marzan, L. M.; Carmie, S.; Chan, D. Y. C.; Mulvaney, P. *Adv. Funct. Mater.* **2004**, *14*, 571.
- (37) Correa-Duarte, M. A.; Pérez-Juste, J.; Sánchez-Iglesias, A.; Giersig, M.; Liz-Marzán, L. M. *Angew. Chem. Int. Ed.* **2005**, *44*, 4375.
- (38) Li, N. B.; Liu, S. P.; Luo, H. Q. *Anal. Lett.* **2002**, *35*, 1229.
- (39) Bahri, M. A.; Hoebeke, M.; Grammenos, A.; Delanaye, L.; Vandewalle, N.; Seret, A. *Colloid Surface A* **2006**, *290*, 206.
- (40) Ding, D.; Liu, K.; He, S.; Gao, C.; Yin, Y. *Nano Lett.* **2014**, *14*, 6731.
- (41) Cushing, S. K.; Bristow, A. D.; Wu, N. *Phys. Chem. Chem. Phys.* **2015**, *17*, 30013.
- (42) Cushing, S. K.; Li, J. T.; Bright, J.; Yost, B. T.; Zheng, P.; Bristow, A. D.; Wu, N. Q. *J. Phys. Chem. C* **2015**, *119*, 16239.
- (43) Costi, R.; Saunders, A. E.; Elmaleh, E.; Salant, A.; Banin, U. *Nano Lett.* **2008**, *8*, 637.
- (44) Cushing, S. K.; Li, J.; Meng, F.; Senty, T. R.; Suri, S.; Zhi, M.; Li, M.; Bristow, A. D.; Wu, N. *J. Am. Chem. Soc.* **2012**, *134*, 15033.
- (45) Hou, W. B.; Hung, W. H.; Pavaskar, P.; Goepfert, A.; Aykol, M.; Cronin, S. B. *ACS Catal.* **2011**, *1*, 929.
- (46) Zhang, Z.; Yates, J. T. *Chem. Rev.* **2012**, *112*, 5520.